

Emission Spectra of Hydrogen-Seeded Helium Arcjets

21 March 2000

Prepared by

R. P. WELLE
Propulsion Science and Experimental Mechanics Department
Space Materials Laboratory
Laboratory Operations

Prepared for

SPACE AND MISSILE SYSTEMS CENTER
AIR FORCE MATERIEL COMMAND
2430 E. El Segundo Boulevard
Los Angeles Air Force Base, CA 90245

Engineering and Technology Group

APPROVED FOR PUBLIC RELEASE;
DISTRIBUTION UNLIMITED

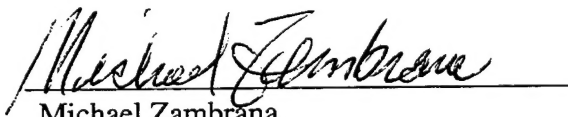
DTIC QUALITY INSPECTED 4

20000815 066

This report was submitted by The Aerospace Corporation, El Segundo, CA 90245-4691, under Contract No. F04701-93-C-0094 with the Space and Missile Systems Center, 2430 E. El Segundo Blvd., Los Angeles Air Force Base, CA 90245. It was reviewed and approved for The Aerospace Corporation by P. D. Fleischauer, Principal Director, Space Materials Laboratory. Michael Zambrana was the project officer for the Mission-Oriented Investigation and Experimentation (MOIE) program.

This report has been reviewed by the Public Affairs Office (PAS) and is releasable to the National Technical Information Service (NTIS). At NTIS, it will be available to the general public, including foreign nationals.

This technical report has been reviewed and is approved for publication. Publication of this report does not constitute Air Force approval of the report's findings or conclusions. It is published only for the exchange and stimulation of ideas.

A handwritten signature in cursive script, reading "Michael Zambrana", is written over a horizontal line.

Michael Zambrana
SMC/AXE

Contents

1.	Introduction and Background.....	1
2.	Previous Helium Arcjet Work	5
3.	Experiment Description.....	6
4.	Experimental Results	7
5.	Summary and Conclusions	13
	References	14

Figures

1.	Grotrian Diagram of the neutral helium atom, from reference 4.....	3
2.	Emission spectrum of the arcjet operating on pure helium.	7
3.	Emission spectrum of the arcjet operating on helium with hydrogen seeded at 5.6% by mass.	8
4.	Emission from the 4^1P-2^1S , 4^1D-2^1P , 4^3P-2^3S , and 4^3S-2^3P lines of helium as a function of hydrogen flow rate.	8
5.	Detail of the emission spectrum of the pure helium arcjet showing several series of emission lines.	9
6.	Representative Boltzmann plot.	9
7.	Plume electron temperature as a function of hydrogen flow rate.	10
8.	Plume electron temperature as a function of axial position.	11
9.	Emission intensity of the 4^1P-2^1S , 4^1D-2^1P , 4^3P-2^3S , and 4^3D-2^3P lines of helium as a function of distance from the nozzle throat, as compared to a $1/r^3$ decay.	11

1. Introduction and Background

Continuing developments in electric propulsion are making it increasingly attractive for satellite operations. Beyond the launch of satellites from the Earth's surface to low Earth orbit, there are two main space propulsion applications; controlling satellite attitude and position, and transferring satellites from one orbit to another.¹ Orbital transfer applications are characterized by one-time velocity changes whose magnitude depends on the orbital parameters of the initial and final orbits. The most common orbital transfer is the transfer from low Earth orbit to geosynchronous Earth orbit, the LEO-to-GEO transfer. Analyses considering the cost of electric power in space and propulsion efficiency usually determine that the optimum specific impulse for the LEO-to-GEO transfer is 1000-1200 seconds.

Electric propulsion options include several different classes of engines, as well as various propellants. Ion engines typically operate with specific impulses in the 3000 to 10000 second range, well above the optimum specific impulse for the LEO to GEO transfer. The Stationary Plasma Thruster (SPT), can operate in the 1500 to 2000 second I_{sp} range, but the efficiency is typically about 50%.² Another disadvantage of the SPT is that the beam is highly divergent, which leads to concerns about spacecraft contamination.³ Arcjets typically operate at specific impulses between 500 and 1200 seconds, with electrical efficiencies of about 50%.

Arcjets operate by heating a gas with an electric arc, and expanding the heated gas through a converging-diverging nozzle to produce thrust. A typical arcjet design is cylindrically symmetric, with a central cathode, and an anode in the shape of a nozzle. A gas flows through the region between the cathode and anode, exhausting through the converging/diverging nozzle to provide thrust. An electric arc is struck between the electrodes, with the anode arc attachment normally downstream of the constriction in the nozzle. The gas is heated either by passing through, or mixing with gas which has passed through, the arc. Arcjets can operate on a variety of propellants. For the LEO-to-GEO transfer, likely propellants include hydrogen and ammonia.^{4,5,6} Helium has also been considered as a propellant for this application because of the potential for much higher efficiency with arcjets operating on helium.

Performance in electric propulsion systems is measured in terms of two parameters, the specific impulse and the electrical efficiency.⁷ The specific impulse (I_{sp}) of an electrothermal rocket is directly proportional to its exhaust speed. To increase exhaust speed, and therefore I_{sp} , arcjets use electric power to heat a propellant, which then undergoes a thermal expansion through a converging-diverging nozzle to accelerate the propellant. The exhaust speed of an ideal thermal expansion through a supersonic nozzle is proportional to $\sqrt{T/M}$ where T is the plenum temperature of the gas, and M is the molecular weight. This proportionality is strictly true only for ideal gases. As the temperature increases, the effects of chemistry, electronic excitation, or ionization will influence the energy available for propulsion. In any case, higher specific impulses are clearly obtained by increasing the temperature and decreasing the molecular weight of the gas. The practical upper limits on temperature are determined by the characteristics of the heat transfer from the gas to the thruster body, and by the properties of the thruster body materials. The practical lower limit on the molecular weight is 1 AMU with atomic hydrogen; this is the reason hydrogen is often the preferred propellant for arcjets.

The electrical efficiency of an arcjet is the ratio between thrust power and electrical input power:

$$\eta = \frac{P_T}{P_e} \quad (1)$$

The thrust power is defined as

$$P_T = \frac{\dot{m}u_e^2}{2} = \frac{F^2}{2\dot{m}} \quad (2)$$

where \dot{m} is the propellant mass flow rate, and u_e is the exhaust speed of a uniform propellant stream which would provide the thrust F . Thus, the efficiency is given by

$$\eta = \frac{F^2}{2P_e\dot{m}} \quad (3)$$

Inefficiencies in arcjet thrusters include any path by which power is lost from the arcjet other than the thrust. Principal paths include heat transfer to the arcjet body which is not recovered by regenerative cooling, nozzle inefficiencies which result in non-directed kinetic energy in the exhaust plume, and frozen flow losses due to atomic or molecular excitation and ionization, and unrecovered dissociation energy. The relative importance of these loss mechanisms depends on the properties of the propellant and on the operating conditions of the arcjet.

Frozen flow losses include electronic, vibrational, and rotational excitation of the exhaust species, as well as any energy which may be required for dissociation. These losses occur because of the failure of atoms, electrons, and ions to recombine and relax during their residence time in the nozzle. The associated energies are not recoverable and are "frozen" into the flow. Under the conditions typical of arcjets, freezing takes place at the throat.⁸ The significance of this loss mechanism depends on the properties of the propellant gas. For a diatomic gas like hydrogen, vibrational and rotational states are excited at relatively low temperatures; as the temperature increases, electronic excitation, dissociation, and ionization will increase. For a monatomic gas such as helium, there are no rotational or vibrational modes, as well as no dissociation. Additionally, with helium, electronic excitation and ionization take place at much higher temperatures than in any other gas, including hydrogen. Because of this, the theoretical frozen flow efficiency of helium is significantly higher than other gases in a specific impulse range of 1000 to 1400 seconds.⁹ Operating at a specific impulse of 1200 seconds, a hydrogen arcjet should have a frozen flow efficiency near 0.4, and this will be the dominant loss mechanism. A combination of experimental and numerical work by Hoskins et. al.¹⁰ showed frozen flow losses in a 10 kW class hydrogen arcjet to be between 30 and 40% of the input power. At the same specific impulse, a helium arcjet should have a frozen flow efficiency above 0.9. Since 1200 seconds is considered an optimum specific impulse for the LEO-to-GEO transfer, helium could have significant potential as a propellant for this application.

Except for ionization, the only frozen flow loss path in the helium arcjet is in electronic excitation of helium atoms. Figure 1 is the Grotrian Diagram of helium showing the energy levels of the various excited states, and the allowed electronic transitions among the lower energy states.¹¹ The 2^1S and 2^3S states have no allowed electronic transitions to lower states, and are termed metastable. The allowed electronic transitions occur with upper state lifetimes short compared to the 1-10 μs residence time of the propellant in the arcjet, while the lifetimes of the two metastable states are long compared to arcjet residence times. One might therefore expect that essentially all of the electronically excited helium atoms in the arcjet plume will be in one of the two metastable states. Continuing emission from the non-metastable states in the plume implies that there is some mechanism operating for

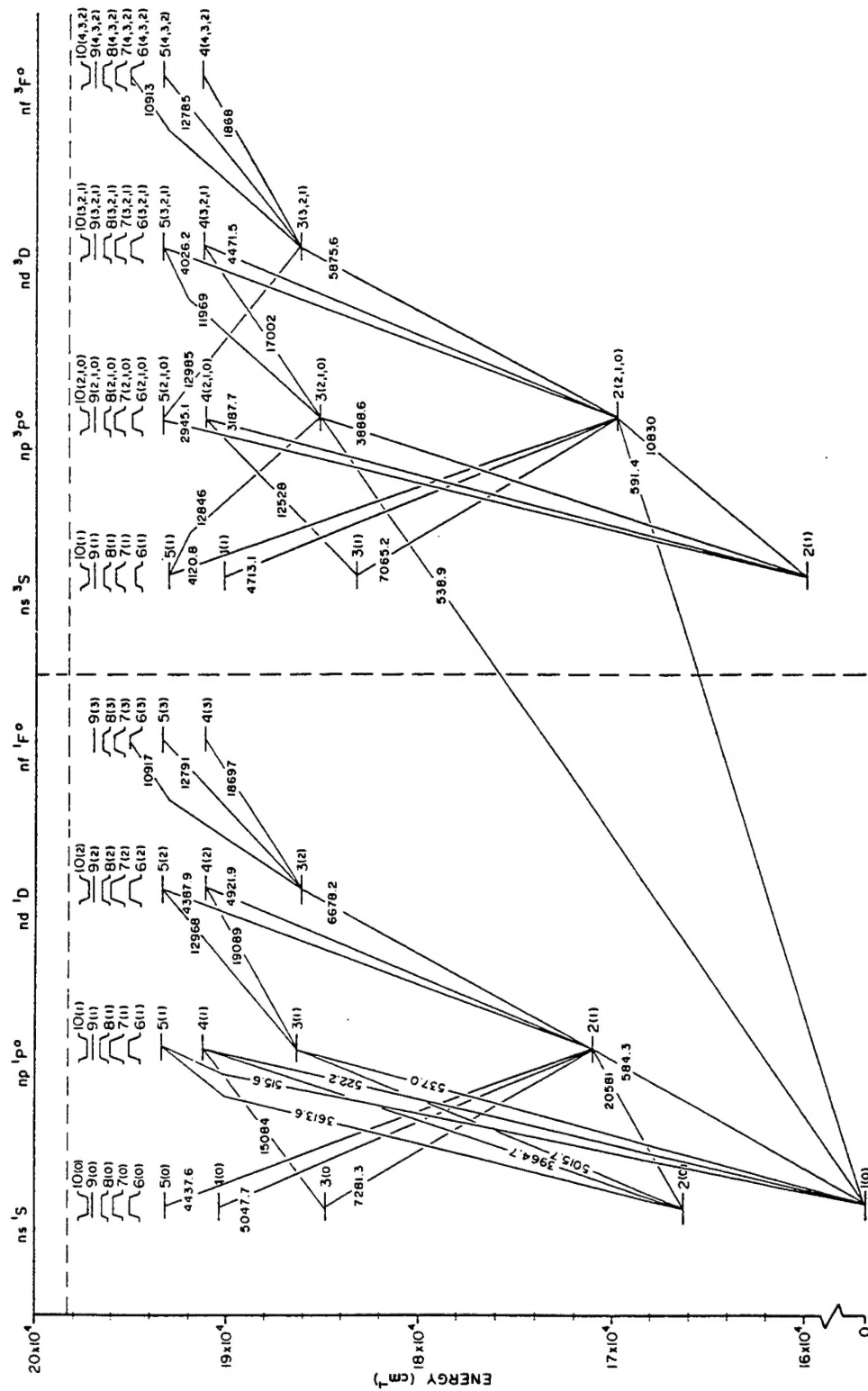


Figure 1. Grotrian Diagram of the neutral helium atom, from reference 11.

repopulating these states at significant distances from the arc. Two possibilities are considered below; excitation through absorption of photons emitted from the arc in the nozzle, or collisional excitation processes.

The energy level of the metastable states is approximately 20.6 eV, while the translational kinetic energy of a helium atom at 10 km/s (corresponding to 1000 seconds I_{sp}) is 2.1 ev. Thus, a metastable fraction of 10^{-3} will correspond to $\sim 1\%$ of the arcjet input energy. Metastable fractions smaller than 10^{-3} will not result in any appreciable frozen flow loss.

2. Previous Helium Arcjet Work

After a small initial effort on helium arcjets in the early 1960's, very little additional work was done to evaluate their potential application, primarily because of propellant storage concerns. These problems appear now to be solvable.¹² Preliminary work in this laboratory¹³ indicated that high efficiency operation of helium arcjets might be possible, but several issues remained to be resolved. The first experiments in this laboratory showed that, in contrast to hydrogen or ammonia, helium arcjets are unstable on time scales ranging from fractions of a second to tens of minutes. Specifically, using a constant mass flow, and a constant current power supply, the measured voltage, power, and thrust of the arcjet fluctuated by up to 40% over periods of seconds to minutes. The cause of the observed instability in helium operation is unknown. On the other hand, hydrogen operation has been observed to be stable within 1% for hours at a time.¹³

It has also been noted during those and subsequent¹⁴ helium arcjet experiments that addition of a small amount (~1%) of hydrogen to the flow had a significant effect on plume appearance as well as on arc stability. In addition, it was thought possible that hydrogen, with its lower ionization potential, might act as the primary current carrier, minimizing excitation of the helium metastable states that are the primary frozen flow loss mechanism of the helium arcjet.

With this background in mind, a set of experiments has been planned to evaluate the utility of helium arcjets for the LEO-to-GEO transfer. An earlier paper¹⁴ reported on a series of experiments in which the effects of arcjet configuration, mass flow rate, and propellant composition were evaluated through measurements of arcjet performance. This paper reports on emission spectra obtained from the plume of an arcjet operating on helium with a hydrogen seeding rate varying from zero to 10% by mass.

3. Experiment Description

These experiments were conducted using an Aerospace manufactured derivative of the NASA-Lewis 1 kW laboratory model arcjet.¹⁵ Power to the arcjet was supplied by a regulated dc source and a nominal 1 kW arc power conditioner supplied by NASA-Lewis. This unit was capable of supplying up to 15 amps to the arc. In this set of experiments, arc current was held constant at 14 amps. Arc voltage varied between about 50 and 80 volts, depending primarily on propellant composition.

Propellant feed to the arcjet is controlled by MKS model 1259B flow meters which operate by monitoring the thermal effects of the flowing gases. In our configuration, the flow is metered upstream of the flow controller, so that the flow meter operates at regulator supply pressure (typically 50 pounds per square inch), independent of arcjet feed pressure. The flow meters are each calibrated for their respective gases by flowing the gas through either a 100 ml or a 1.0 liter bubble meter, depending on flow rate, downstream of the flow meters and flow controllers.

These experiments were conducted in a vacuum chamber of 0.5 m diameter and 1 m length. The arcjet exhaust was pumped through a diffuser to a roots blower backed by a roughing pump. The vacuum chamber was also pumped by a set of roughing pumps. Chamber pressure during these experiments was typically about two torr.

Emission spectra were obtained by imaging the centerline of the plume of the arcjet onto the entrance slit of a GCA/McPherson model 2051 spectrograph. The exit slit of the spectrograph was imaged by a Princeton Instruments liquid nitrogen cooled ccd array having 298 by 1151 25 μm pixels. For this experiment the array was operated at a temperature of -80 C. The array was oriented relative to the exit slit such that each pixel on the short axis of the array corresponded to a distance of 0.43 mm on the axis of the arcjet plume. With a 150 lines/mm grating in place in the spectrograph, each pixel on the long axis of the ccd array corresponded to a wavelength interval of 0.22 nm. Wavelength calibration for a given set of images was provided by assigning the known lines of the helium spectrum. This configuration provided for the simultaneous acquisition of emission spectra at a number of positions along the axis of the plume.

4. Experimental Results

In the current set of experiments, particular attention was paid to the effect of hydrogen seeding. The hydrogen seeding resulted in changes in plume appearance similar to those noted earlier; a significant reduction in the overall optical emission from the plume, and a change of color from yellow toward red. The color change can be attributed to a shift from helium to hydrogen as the dominant emitter, which occurs as the hydrogen fraction is increased. Figures 2 and 3 show survey spectra of the emission from the plume for two cases. In the first case, the propellant is pure helium, while in the second case, hydrogen is seeded at 5.6% by mass. The figures show the spectra plotted on a log scale on the intensity axis in order to bring out some of the details of the weaker lines.

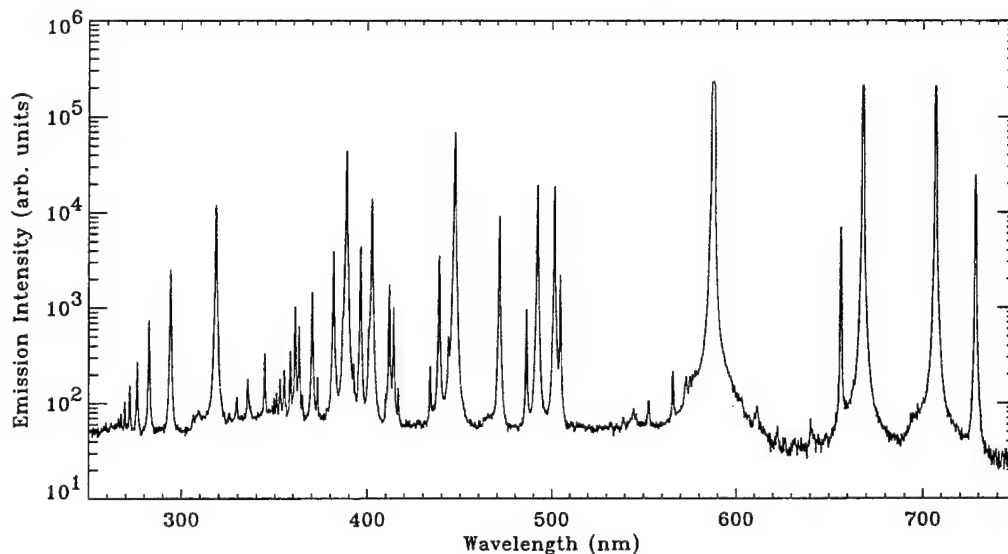


Figure 2. Emission spectrum of the arcjet operating on pure helium.

In the pure helium case, the lines are, in all but a few cases, assignable to atomic helium transitions. Indeed, several series of lines corresponding to certain lower energy levels are easily identifiable. The few lines not attributable to helium atomic transitions can be assigned to the hydrogen Balmer series. These probably arise from residual hydrogen or water contaminating the system. In the second spectrum, with hydrogen seeding at 5.6% by mass, the atomic helium emission is reduced by two orders of magnitude relative to the pure helium case, and the spectrum is dominated by the hydrogen Balmer series.

This effect is further illustrated in Figure 4 where the intensity of four lines in the helium emission spectrum are plotted as a function of hydrogen concentration. The four spectral lines used to generate Figure 4 are 4^1P-2^1S at 396.5 nm, 4^1D-2^1P at 492.2 nm, 4^3P-2^3S at 318.8 nm, and 4^3S-2^3P at 471.3 nm. Except for the 4^1P-2^1S line at 396.5 nm, all lines decrease to less than a few percent of their original intensity with the addition of 5% hydrogen. As the hydrogen concentration is increased, the intensity of the helium 4^1P-2^1S line is overwhelmed by the hydrogen Balmer- ϵ line ($n=7$) at 397.0 nm.

Figure 5 shows expanded detail on the spectrum of the pure helium case. In this figure, six series of

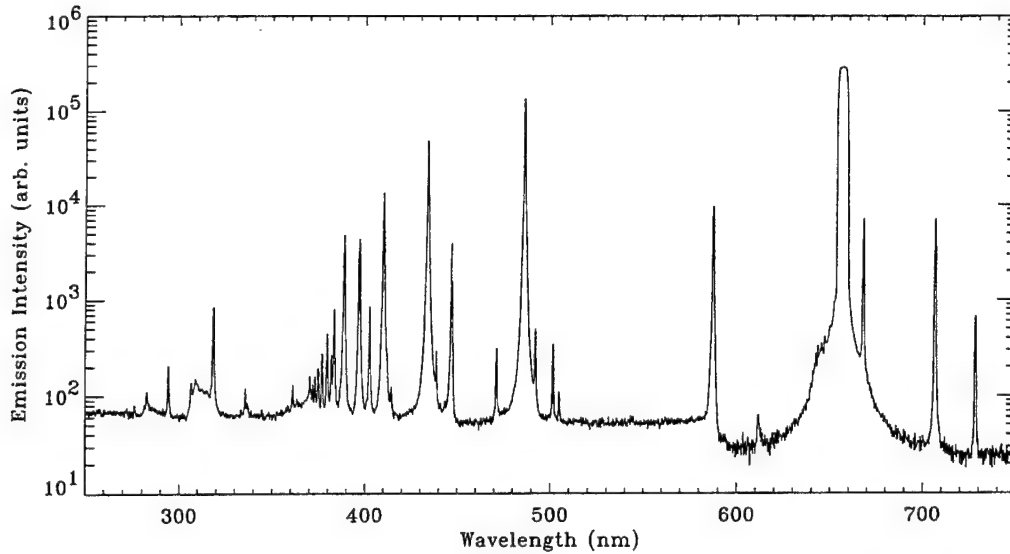


Figure 3. Emission spectrum of the arcjet operating on helium with hydrogen seeded at 5.6% by mass.

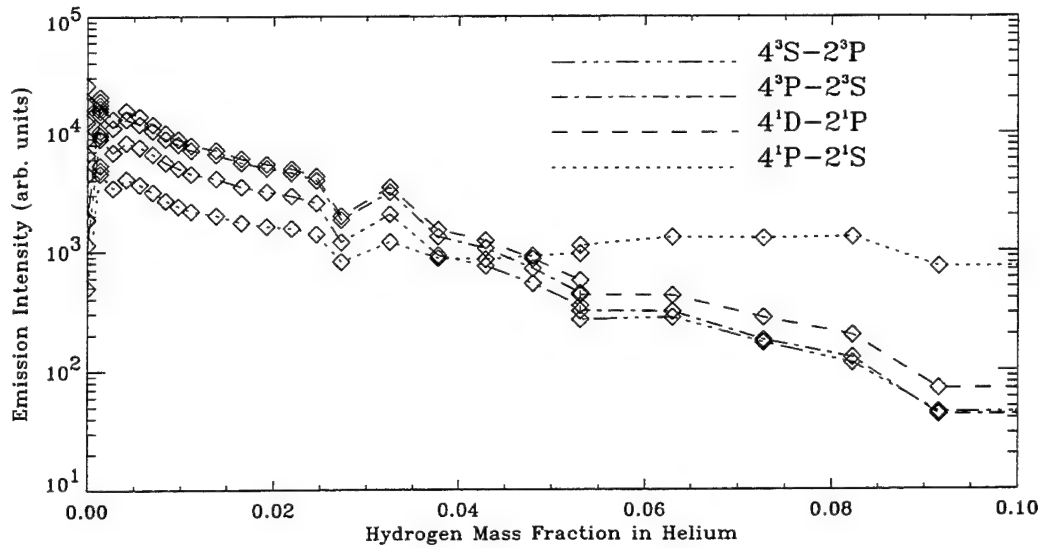


Figure 4. Emission from the 4^1P-2^1S , 4^1D-2^1P , 4^3P-2^3S , and 4^3S-2^3P lines of helium as a function of hydrogen flow rate.

lines are identified, corresponding to the transitions n^3P-2^3S , n^1P-2^1S , n^3D-2^3P , n^1D-2^1P , n^1S-2^1P , and n^3S-2^3P .

In the spectrum shown in Figure 5, the $n=4,5,6,7,8$ lines in the n^3P-2^3S series are strong enough and sufficiently well defined to allow an electron temperature to be determined using the method of the Boltzmann plot. This method is derived from the expression for the intensity of a spectral line

$$I = \frac{2\pi hc^2 r_0}{\lambda^3} g f N_0 e^{-E_u/kT} \quad (4)$$

where h is Planck's constant, c is the speed of light, r_0 is the electron radius, λ is the wavelength

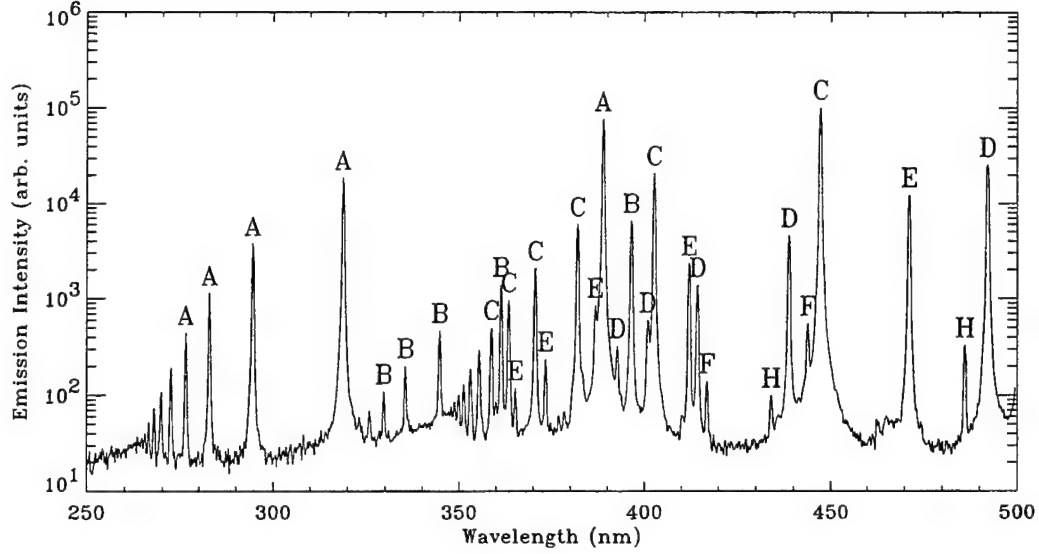


Figure 5. Detail of the emission spectrum of the pure helium arcjet showing several series of emission lines labeled as follows: A, n^3P-2^3S ; B, n^1P-2^1S ; C, n^3D-2^3P ; D, n^1D-2^1P ; E, n^3S-2^3P ; and F, n^1S-2^1P . The two lines labeled H at 434.0 and 486.3 nm are the $n=5$ and $n=4$ lines of the hydrogen Balmer series.

of the line, g is the statistical weight of the lower energy level, f is the oscillator strength, N_0 is the total atom density, E_u is the energy of the upper state, k is Boltzmann's constant, and T is the electron temperature. By plotting E_u against $k \ln(I\lambda^3/fg)$ one obtains a line with the slope of $-1/T$.

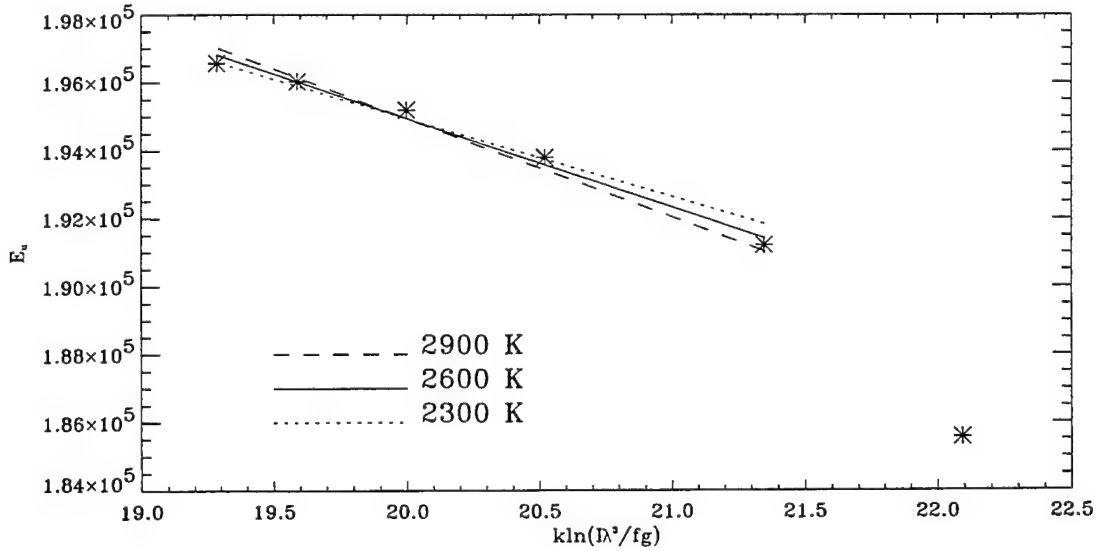


Figure 6. Representative Boatsman plot. The least-squares best fit straight line corresponds to a temperature of 2608 K in this case. The lines corresponding to 2300 K and 2900 K are shown to provide an estimate of the uncertainty in the calculation.

A representative plot is shown in Figure 6. The data point for the $n=3$ line is also shown, but it is

not used in determining the best fit straight line. It appears to fall well below the line which fits the $n=4,5,6,7,8$ points, which is probably due to self absorption of the $n=3$ line in the plume. The current experiment does not provide sufficient spectral resolution to make meaningful measurements of line shapes, so self absorption cannot be easily evaluated. Future plans include these line shape measurements. The electron temperature indicated by the slope of the best fit line in Figure 6 is 2608 K. A ± 300 K estimate of the uncertainty of this measurement is obtained by plotting lines corresponding to temperatures of 2300 and 2900 K on the same figure.

With the available data, electron temperatures can be determined as a function of hydrogen concentration in the propellant, and as a function of position along the axis of the plume. Figure 7 shows the temperature of the plume as a function of hydrogen concentration, as determined from the $n=4,5,6,7$ lines of the n^3P-2^3S series. With pure helium, the arcjet operation tends to be somewhat unstable, leading to a large scatter in the temperature reading. On the other hand, as the hydrogen concentration increases, the emission from these lines decreases, making the temperature determination more uncertain. To improve the signal-to-noise ratio, data were averaged over the first 7.5 mm beyond the exit plane of the nozzle. Within the uncertainty limits, there appears to be no measurable difference in plume temperature as a function of hydrogen concentration.

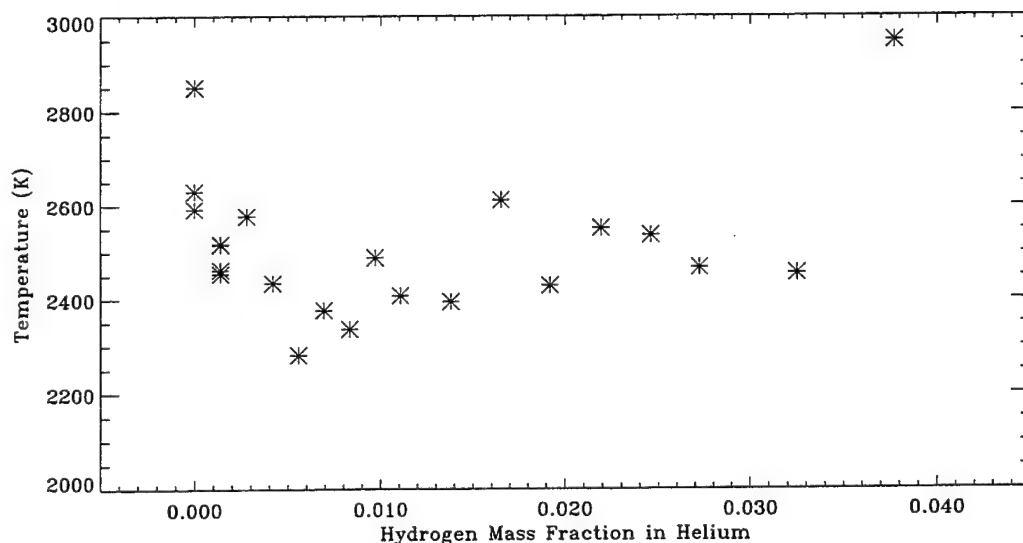


Figure 7. Plume electron temperature as a function of hydrogen flow rate.

Similarly, the temperature of the plume for a given operating condition can be determined as a function of distance from the exit plane. In this case, the data become more uncertain with increasing distance from the exit plane because of the decrease in emission intensity. Figure 8 shows the temperature of the plume as a function of distance for an arcjet operating on pure helium. The scatter in the data gives an indication of the uncertainty of the measurement. Within this uncertainty, there is no obvious trend toward a change in plume temperature with distance.

In addition to the temperature of the plume, one can obtain useful information by observing the rate at which the plume emission intensity falls off as a function of distance from the throat of the arcjet. The four lines used to generate Figure 4 are used again in Figure 9. In this case, the intensities of the lines as a function of distance from the throat are shown for a case using pure helium. Also shown on Figure 9 is a solid line illustrating a $1/r^3$ decay in intensity. It is seen that the four lines

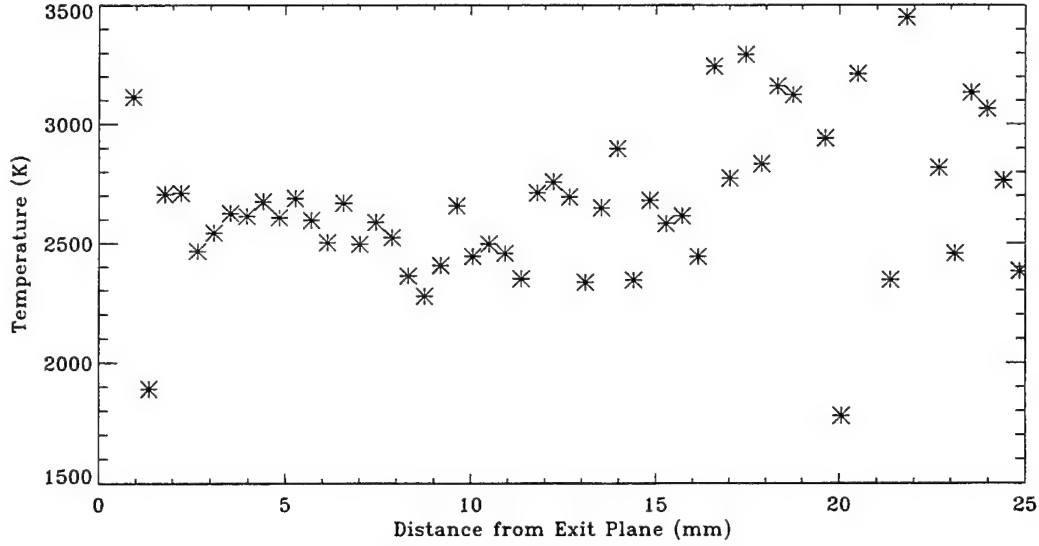


Figure 8. Plume electron temperature as a function of axial position.

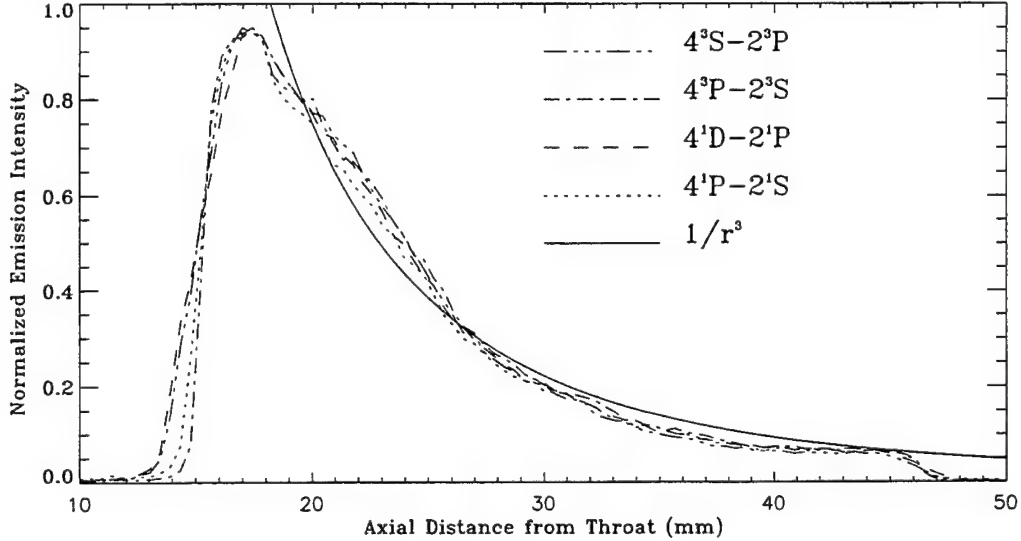


Figure 9. Emission intensity of the 4^1P-2^1S , 4^1D-2^1P , 4^3P-2^3S , and 4^3D-2^3P lines of helium as a function of distance from the nozzle throat, as compared to a $1/r^3$ decay.

all decay at approximately the same rate, and that this is approximately a $1/r^3$ dependence.

In order to understand the significance of this result, one needs to consider several factors. First, the imaging system used to obtain the spectra sees essentially a thin slice, or plane, which contains the axis of the arcjet. Second, the expansion of the plume in this region is essentially conical. These two factors combined should result in a $1/r$ dependence for the number of atoms seen by the imaging system. On the other hand, the further decrease in emission intensity cannot be explained by a simple decay in the number density of the excited states due to electronic emission. The lifetimes of the upper states for these four lines are on the order of 10 ns, during which time the atoms will travel no more than 50 micrometers. Since the plume persists over a distance of 10's of millimeters, some mechanism must be repopulating the upper states as the plume expands. Two possibilities are

considered, photo-excitation due to absorption of photons emitted from the arc in the nozzle of the arcjet, and collisional excitation involving free electrons in the plume. Atom-atom collisions can be neglected because of the much lower mobility of the atoms relative to the electrons. Photo-excitation requires, in addition to photons of appropriate energies, a reservoir of atoms in states which can be optically coupled to the excited states. The four emission lines used to generate figure 9 originate from the 4^1P , 4^1D , 4^3P , and 4^3D states. The possible reservoirs of atoms which could be photo-excited would include ground state helium and the two metastable states. Reference to the Grotrian diagram in Figure 1 shows that the 4^1P , and 4^3P states can each be optically coupled to one of the metastable states. In addition, the 4^1P state can be optically coupled to the ground state. On the other hand the D states cannot be directly coupled to either the ground or metastable states, and could only be photo-excited through an intermediary state. As such, if the excited state population were being maintained through photo-excitation from the direct arc emission, the emission lines originating on the D states would be expected to decay more rapidly with plume expansion than would the emission lines originating on the P states. The observation that they decay at the same rate implies that another mechanism must be operating.

That the excited state population is maintained by a collisional process is further implied by the $1/r^3$ decay rate. Because the plume is expanding in a conical manner, the absolute number density of atoms in the plume should fall as $1/r^2$. The collision rate should be proportional to the number density. This $1/r^2$ factor, combined with the $1/r$ factor derived from the imaging system, leads to the expectation that the emission intensity of the helium lines should fall as $1/r^3$ where r is the distance from the throat of the arcjet. Note that the throat is the appropriate reference point as this is the apex of the conical expansion which leads to both the $1/r$ and the $1/r^2$ factors.

5. Summary and Conclusions

As discussed above, the observation that the emission from the plume falls as $1/r^3$ with the distance from the throat of the nozzle implies that the population of the electronically excited helium states in the plume is controlled by a collisional process. Since the lifetimes of the non-metastable states are short compared to the transit time through the plume, they should be in thermal equilibrium with the metastable states and the electrons in the plume, and the number density of the excited states should be directly proportional to the number density of the metastable states. Since the emission falls as $1/r^3$, there appears to be no significant mechanism for de-excitation of the metastable states beyond the exit plane of the nozzle.

The second principal observation of this experiment is that the introduction of hydrogen seeding results in a very large decrease in the emission from the upper excited helium states. As the upper electronic states of helium are apparently maintained in thermal equilibrium with the metastable states through electron collisions, the decrease in visible emission from the excited helium lines with increasing hydrogen concentration would imply a corresponding decrease in the number density of both the upper excited states and the metastable states.

On the other hand, one would expect that this reduction in metastables would have some effect on the electron temperature of the plume, which is not observed. In addition, since the metastable states carry about 20 eV of energy, it might be expected that the decrease in the metastable number density would affect the electrical efficiency of the arcjet. This was not observed in earlier work.¹⁴ One possibility is that the decrease in frozen flow loss to the metastables is taken up in frozen flow loss to the hydrogen, through dissociation, and ionization. An alternative possibility is that the total number density of metastables in the plume is small enough that even in the pure helium arcjet, they do not contribute significantly to the frozen flow. Further experiments will be required to determine the actual metastable number density in the plume.

As with the previous performance studies, hydrogen seeding cannot yet be completely discounted as a method of improving the utility of helium arcjets. In this work, although there was an apparent large decrease in the number of helium metastables with increasing hydrogen flow, there was no change in plume temperature. In the earlier work, hydrogen seeding at about 1% by mass did contribute to arc stability under almost all operating conditions. On the other hand, the trends were toward a smaller effect as propellant flow rates and cathode gaps were increased, and hydrogen seeding may be unnecessary with the configurations, power levels, and flow rates appropriate for space propulsion applications.

Further information about the frozen flow loss mechanisms in the helium and hydrogen-seeded helium arcjet may be obtained through additional optical diagnostic methods, including higher resolution emission spectroscopy to obtain line shapes, which are an indicator of electron number densities, and atomic absorption studies to directly measure the number densities of the helium metastables.

References

- 1 S.W. Janson, "The On-Orbit Role of Electric Propulsion," AIAA-93-2220, 29th Joint Propulsion Conference, June 1993.
- 2 Charles E. Vaughan and R. Joseph Cassady, "An Updated Assessment of electric Propulsion Technology for Near-Earth Space Missions," AIAA-92-3202, 28th Joint Propulsion Conference, July 1992.
- 3 Roger M. Myers and David H. Manzella, "Stationary Plasma Thruster Plume Characteristics," IEPC Paper 93-096 in *Proceedings of the 23rd International Electric Propulsion Conference*, September 1993.
- 4 K.P. Zondervan, A.K. Chan, C.A. Feuchter, and W.B. Smith, "Operational Requirements for Cost Effective Payload Delivery with Solar Electric Propulsion," IEPC-93-203, Presented at the 23rd International Electric Propulsion Conference, September 1993.
- 5 T.M. Miller, and G.B. Seaworth, "Mission Factors Affecting Cost Optimization of Solar Electric Orbital Transfer Vehicles," IEPC-93-202, Presented at the 23rd International Electric Propulsion Conference, September 1993.
- 6 T.M. Miller, "Systems Analysis for an Operational EOTV," IEPC-91-133, *Proceedings of the 22nd International Electric Propulsion Conference*, October 1991.
- 7 R.G. Jahn, *The Physics of Electric Propulsion*, McGraw-Hill, 1968.
- 8 Lewis E. Wallner and Joseph Czika, Jr., "Arc-Jet Thrustor for Space Propulsion," NASA TN D-2868, June 1965.
- 9 John R. Jack, "Theoretical Performance of Propellants Suitable for Electrothermal Jet Engines," *ARS Journal*, December 1961, pp 1685-9.
- 10 W.A. Hoskins, A.E. Kull, W.M. Nesser, and G.W. Butler, "Measurement of Energy Deposition Modes in an Intermediate Power Hydrogen Arcjet," IEPC Paper 93-216 in *Proceedings of the 23rd International Electric Propulsion Conference*, September 1993.
- 11 Stanley Bashkin and John O. Stoner, Jr., *Atomic Energy Levels & Grotrian Diagrams*, North-Holland Publishing Company, 1975.
- 12 R.P. Welle "Propellant Storage Considerations for Electric Propulsion," IEPC-91-107, *Proceedings of the 22nd International Electric Propulsion Conference*, October 1991.
- 13 R.P. Welle, J.E. Pollard, S.W. Janson, M.W. Crofton, and R.B. Cohen, "One Kilowatt Hydrogen and Helium Arcjet Performance," AIAA-91-2229, 27th Joint Propulsion Conference, June 1991.
- 14 R.P. Welle, "Space Propulsion Applications of Helium Arcjets," AIAA-97-0794, 35th Aerospace Sciences Meeting, January 1997.
- 15 F.M. Curran and T.W. Haag, "An Extended Life and Performance Test of a Low Power Arcjet," AIAA-88-3106, 24th Joint Propulsion Conference, July 1988.

LABORATORY OPERATIONS

The Aerospace Corporation functions as an "architect-engineer" for national security programs, specializing in advanced military space systems. The Corporation's Laboratory Operations supports the effective and timely development and operation of national security systems through scientific research and the application of advanced technology. Vital to the success of the Corporation is the technical staff's wide-ranging expertise and its ability to stay abreast of new technological developments and program support issues associated with rapidly evolving space systems. Contributing capabilities are provided by these individual organizations:

Electronics and Photonics Laboratory: Microelectronics, VLSI reliability, failure analysis, solid-state device physics, compound semiconductors, radiation effects, infrared and CCD detector devices, data storage and display technologies; lasers and electro-optics, solid state laser design, micro-optics, optical communications, and fiber optic sensors; atomic frequency standards, applied laser spectroscopy, laser chemistry, atmospheric propagation and beam control, LIDAR/LADAR remote sensing; solar cell and array testing and evaluation, battery electrochemistry, battery testing and evaluation.

Space Materials Laboratory: Evaluation and characterizations of new materials and processing techniques: metals, alloys, ceramics, polymers, thin films, and composites; development of advanced deposition processes; nondestructive evaluation, component failure analysis and reliability; structural mechanics, fracture mechanics, and stress corrosion; analysis and evaluation of materials at cryogenic and elevated temperatures; launch vehicle fluid mechanics, heat transfer and flight dynamics; aerothermodynamics; chemical and electric propulsion; environmental chemistry; combustion processes; space environment effects on materials, hardening and vulnerability assessment; contamination, thermal and structural control; lubrication and surface phenomena.

Space Science Applications Laboratory: Magnetospheric, auroral and cosmic ray physics, wave-particle interactions, magnetospheric plasma waves; atmospheric and ionospheric physics, density and composition of the upper atmosphere, remote sensing using atmospheric radiation; solar physics, infrared astronomy, infrared signature analysis; infrared surveillance, imaging, remote sensing, and hyperspectral imaging; effects of solar activity, magnetic storms and nuclear explosions on the Earth's atmosphere, ionosphere and magnetosphere; effects of electromagnetic and particulate radiations on space systems; space instrumentation, design fabrication and test; environmental chemistry, trace detection; atmospheric chemical reactions, atmospheric optics, light scattering, state-specific chemical reactions and radiative signatures of missile plumes.

Center for Microtechnology: Microelectromechanical systems (MEMS) for space applications; assessment of microtechnology space applications; laser micromachining; laser-surface physical and chemical interactions; micropropulsion; micro- and nanosatellite mission analysis; intelligent microinstruments for monitoring space and launch system environments.

Office of Spectral Applications: Multispectral and hyperspectral sensor development; data analysis and algorithm development; applications of multispectral and hyperspectral imaging to defense, civil space, commercial, and environmental missions.



2350 E. El Segundo Boulevard
El Segundo, California 90245-4691
U.S.A.